Intermediate Temperature Fuel Cells via an Ion-Pair Coordinated Polymer Electrolyte

Journal:	*Energy & Environmental Science*
Manuscript ID	EE-ART-12-2017-003595.R3
Article Type:	Paper
Date Submitted by the Author:	28-Feb-2018

Complete List of Authors:	Lee, Kwan Soo; Los Alamos National Laboratory, Maurya, Sandip; Los Alamos National Laboratory, MPA-11: Materials Synthesis and Integrated Devices Kim, Yu Seung; Los Alamos National Laboratory, Kreller, Cortney; Los Alamos National Lab, MPA11 Wilson, Mahlon; Los Alamos National Laboratory, Sensors and Electrochemical Devices Group Larsen, Dennis; Ceramatec Inc; Oxeonenergy Elangovan, S.; Ceramatec, Inc, Mukundan, Rangachary; Los Alamos National Laboratory,

Energy & Environmental Science

ARTICLE

Intermediate Temperature Fuel Cells via an Ion-Pair Coordinated Polymer Electrolyte

Received 00th January 20xx,
Accepted 00th January 20xx

DOI: 10.1039/x0xx00000x

www.rsc.org/

Kwan-Soo Lee,†[a] Sandip Maurya,[a] Yu Seung Kim,*[a] Cortney R. Kreller,[a] Mahlon Wilson,[a] Dennis Larsen,[b] S. Elango Elangovan,[b] and Rangachary Mukundan*[a]

Fuel cells are attractive devices that convert chemical energy into electricity through the direct electrochemical reaction of hydrogen and oxygen. Intermediate temperature fuel cells operated at 200–300 °C can simplify water and thermal managements, enable the use of non-precious or low-loading precious metal catalysts and provide insensitivity toward fuel and air impurities such as carbon monoxide. However, the performance of current intermediate temperature fuel cells is poor due to a lack of highly-conductive membrane electrolytes and optimal electrodes designed for these fuel cells. Here, we demonstrate high-performing intermediate temperature fuel cells that use SnP_2O_7-polymer composite membranes and a quaternary ammonium-biphosphate ion-pair coordinated polymer electrolyte in the electrodes. The peak power density of the fuel cell under H_2 and O_2 reached 870 mW cm^{-2} at 240 °C with minimal performance loss under exposure to 25% carbon monoxide.

Introduction

Fuel cells are promising electrochemical energy devices that efficiently convert chemical energy in fuels directly to electrical energy. The energy density of chemical fuels used in fuel cells will always be multiple times higher that of the secondary batteries such as lithium-ion, lithium-sulfur, metal-ion and metal-air,[1-3]. Different types of solid electrolyte fuel cells have been developed over the past several decades. At an operating temperature < 100 °C, alkaline membrane fuel cells (AMFCs) or low temperature proton exchange membrane fuel cells (LT-PEMFCs) or using ion-conducting polymer electrolytes have been developed for transportation and stationary applications. State-of-the-art AMFCs and LT-PEMFCs showed excellent performance, *ca.* 500–1000 mW cm^{-2} peak power density under H_2/air.[4,5] The low operating temperatures of AMFCs and LT-PEMFCs make heat removal a challenge and result in large radiator volume. In addition, high material cost and complex water management of the fuel cells hamper further cost reduction and durability improvement of the fuel cells. At a higher operating temperature of 100–200 °C, high temperature proton exchange membrane fuel cells (HT-PEMFCs) using phosphoric acid-doped polybenzimidazole (PBI) electrolytes perform well without external humidification, *ca.* 500–800 mW cm^{-2} peak power density under H_2/air.[6] The operating temperatures of HT-PEMFCs are limited by loss of the weakly bound phosphoric acid when fuel cells are exposed to water below 140 °C or operated > 200 °C. High temperature fuel cells such as protonic ceramic fuel cells (PCFCs) operating at temperature ≥ 350 °C, or solid oxide fuel cells (SOFCs) operating at temperatures > 800 °C achieve power densities of 1400 mW cm^{-2} at 700 °C and 2000 mW cm^{-2} at 900 °C under H_2/air, respectivley.[7-9] However, the fuel cell performance of high temperature fuel cells at low temperatures is poor, ca. ~100 mW cm^{-2} at 350 °C. The operating temperature range of intermediate temperature fuel cells (ITFCs) (200–300 °C) gives benefits over both lower and higher fuel cell operating temperatures. Compared with fuel cells operated at lower temperatures, ITFCs are less poisoned by reactant impurities, such as carbon monoxide or sulfur dioxide,[10] and also have the advantage of minimizing issues related to liquid components such as water management, acid leaking and electrode flooding.[11] Compared with fuel cells operated at higher temperatures, ITFCs have broad material options and compact stack design; thus, offering a path towards lower costs.

Cesium dihydrogen phosphate solid acid, CsH_2PO_4, the most studied electrolyte for ITFCs, has reasonably good conductivity (> 10 mS cm^{-1}) when heated to temperatures between 160 and 250 °C which is accompanied by a melting and phase transition from monoclinic (low temperature) to cubic (high temperature).[9, 12-14] The proton conductivity can further increase to 66 mS cm^{-1} at 272 °C with incorporation of supporting materials such as SiO_2 and SiP_2O_7.[15] Another promising electrolyte for ITFCs is based on metal diphosphates (MP_2O_7, where M = Sn, Ce, and Zr).[16-21] The excellent anhydrous proton conductivity (~10^{-1} S cm^{-1} at temperatures of 150–350 °C) of un-doped and indium-doped SnP_2O_7 was first reported a little over a decade ago.[16, 17] While the promising conductivity

[a] MPA-11: Materials Synthesis and Integrated Devices, Los Alamos National Laboratory, Los Alamos, New Mexico 87545, USA.
[b] Ceramatec, Inc., 2425 South 900 West, Salt Lake City, UT 84119-1517, USA.
† Present address: C-CDE: Chemical Diagnostics and Engineering, Los Alamos National Laboratory, Los Alamos, NM 87545, USA.
‡ Electronic Supplementary Information (ESI) available: See DOI: 10.1039/x0xx00000x

generated a great deal of interest, debate persisted in the literature regarding the conduction mechanism.[17, 22-27] Recent studies on indium-doped and undoped SnP_2O_7 have shown that the crystalline phase itself possesses negligible protonic conductivity, even at temperatures up to 900 °C.[28] Rather, it is an excess amorphous grain boundary polyphosphate phase formed under relatively low processing temperatures (500–700 °C) that is responsible for the protonic conductivity.[29] Thus, the proton conductivity of MP_2O_7 increases as phosphorous to metal (P:M) molar ratio increases. (*e.g.* the proton conductivity of indium-doped SnP_2O_7 increased from 3.2×10^{-5} to 1.0×10^{-2} S cm^{-1} at 250 °C as the P:M ratio increased 2.23 to 2.81[29]) Nevertheless, unlike CsH_2PO_4, which undergoes a phase transformation, no such phase transition is required to achieve good proton conductivity in the metal diphosphate based materials. This offers the advantage of a greater temperature range of functionality with increased power density throughout start-up over cesium dihydrogen phosphate.

While prior works have demonstrated the high conductivity and stability of metal phosphates,[29, 30] the power outputs of ITFCs reported to date are not yet competitive with other types of fuel cells (Fig. 1). The highest reported peak power density of ITFCs using SnP_2O_7 is 264 mW cm^{-2} at 250 °C under H_2/air.[16] A similar performance level has been reported with ITFCs using CsH_2PO_4 (*e.g.* peak power density of ~ 415 mW cm^{-2} at 250 °C under H_2/O_2), in which subsequent performance loss was observed due to the mechanical failure of the thin membrane.[35-37]

Two key limitations to reaching higher and stable power output have been identified. Firstly, the fabrication of robust membrane electrode assemblies (MEAs) containing highly conductive thin membranes is challenging. The MEAs prepared with pressed or slurry-deposited pellets have limited mechanical properties and are prone to leaking of the reactant gases, which cause rapid cell voltage loss.[38] Secondly, the formation of optimum three-phase interfaces at the electrodes enabling fast reactants' access and efficient electrochemical reaction is difficult to obtain with metal phosphate electrolytes.[10] The electrodes containing CsH_2PO_4 or MP_2O_7 particles suffer from a lack of a percolating ion-conducting network in the presence of electrocatalysts and electron-conducting supporting materials. In addition, maximizing the active electrochemical surface area by evenly-coating the catalyst material on the electrolyte particles typically requires high Pt loading, *ca.* > 1 mg_{Pt} cm^{-2}.[39]

Here, we report advances that address both of these limitations, leading to good ITFC performance at temperatures of 200 to 240 °C. For the electrolyte, we prepared SnP_2O_7 powders having a high P:M ratio *via* the solution precipitation method.[29] The relatively low maximum temperature of 650 °C used in this synthesis route can reduce the loss of the phosphate phase and provide good control of the final stoichiometry. The electrolyte separator was prepared from a polymer composite with 90 wt% SnP_2O_7 and 10 wt% perfluorinated Nafion® polymer. In order to maximize the mechanical properties of the highly hygroscopic electrolyte particle concentrated composite membranes, we cast the composite membranes from non-aqueous 1,2-pentanediol dispersion which enhances the polymer chain entanglement during the dispersion-cast process.[40] The fuel cell electrodes were fabricated with quaternary ammonium-biphosphate ion-pair coordinated ionomeric binder, which forms a good three-phase interface between the polymer electrolyte, catalyst and carbon supporting materials. The H_2/O_2 and H_2/air fuel cell performance and CO tolerance are reported.

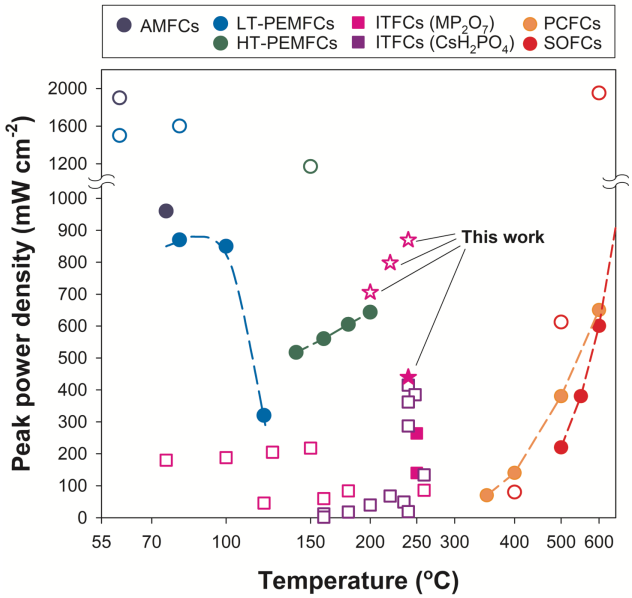

Fig. 1 Performance comparison of different type of fuel cells; filled symbol: H_2/air; unfilled: H_2/O_2. Fuel cell data are taken from references: AMFCs[5, 31]; LT-PEMFCs[4, 32]; HT-PEMFCs[33]; SAFCs[12]; ITFCs[16, 34]; PCFCs and SOFCs[6, 34].

Results and discussion

SnP_2O_7 Powder Preparation

The SnP_2O_7 powders were synthesized *via* the solution precipitation method at 650 °C. A powder was prepared with a P:M ratio of 3.5 (*e.g.* an excess amorphous polyphosphate phase with phosphorous content 1.5× that of the stoichiometric SnP_2O_7) as measured by X-ray fluorescence. Whole profile fitting of the diffraction pattern (Fig. S1, ESI†) measured via X-ray diffraction yielded a crystallite size of 49.6 nm and lattice parameter of ~7.940 Å. No systematic correlation of lattice parameters with excess phosphorous content was observed, indicative of constant P and Sn site occupancies within the crystalline phase in agreement with our previous findings on indium-doped SnP_2O_7.[29] The proton conductivity of an SnP_2O_7 pellet with P:M ratio of 3.5 was measured at 200 °C under H_2/O_2 as a function of time (Fig. S2, ESI†). The proton conductivity of ~100 mS cm^{-1} was stable over 1,400 h of operation in both dry and wet (water partial vapor pressure of 4 kPa) conditions.

Preparation of SnP_2O_7-Nafion Composite Membrane

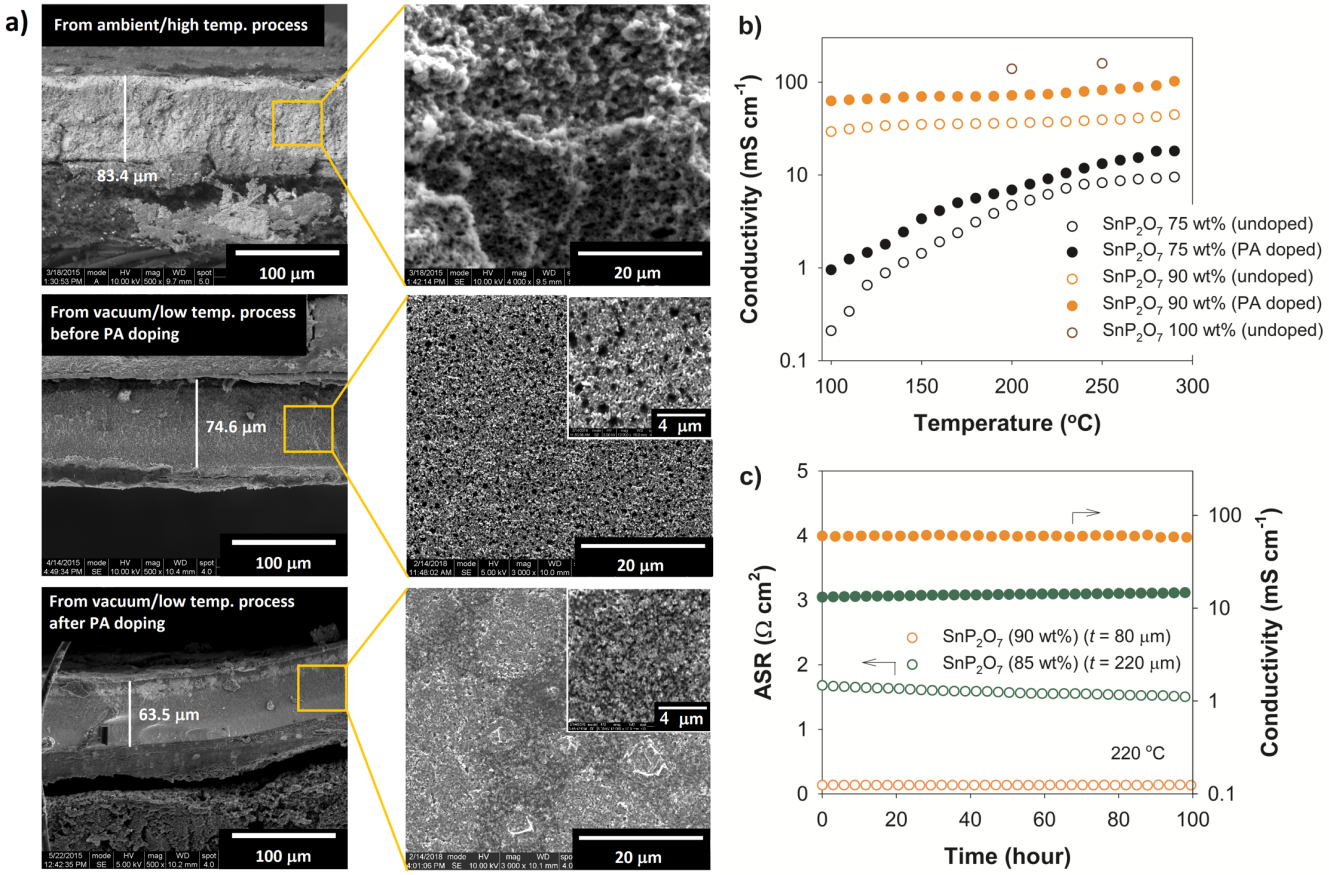

Fig. 2 (a) Scanning electron microscope image of SnP_2O_7-Nafion composite membranes; MEA using SnP_2O_7-Nafion composite prepared from ambient pressure dry at 190 °C (top), The composite membrane prepared from the vacuum dry at 160 °C (middle), The composite membrane prepared from vacuum dry at 160 °C after PA doping (bottom) (b) In-plane proton conductivity of PA doped and un-doped SnP_2O_7-Nafion composite membranes under dry conditions as a function of temperature. (c) Area specific resistance (ASR) and through-plane proton conductivity of phosphoric acid doped SnP_2O_7 -Nafion composite membranes at 220 °C as a function of time.

Polymer composite thin films were prepared using the 3.5 P:M SnP_2O_7 powder in order to reduce the cell ohmic resistance and fabricate robust films. The polymer matrix for the composite membranes requires high thermal stability and mechanical toughness. While high temperature thermoplastic polymers such as Radel® polysulfone limit the concentration of SnP_2O_7 to < 80 wt% due to lack of elongation of the composite membrane, dispersion-cast perfluorinated Nafion® cast membrane from 1,2-pentanediol dispersion enabled incorporation of SnP_2O_7 as high as 93 wt%, while maintaining mechanical integrity of the composite membrane (Fig. S3, ESI†). Our previous study indicated that the relatively long alkyl chain of the dispersing agent enhances the chain entanglement of the perfluorinated polymers to provide the best mechanical toughness[40], *ca.* ~3 times greater tensile toughness than commercially available perfluorinated Nafion polymer (Fig. S4, ESI†).

Fig. 2a shows the SEM images of 90 wt% SnP_2O_7-Nafion composite membranes. The low magnification images of the MEAs show that the 64–84 μm-thick composite membranes were intact between two electrodes. While the composite membrane cast from the ambient pressure at 190 °C created 0.3 to 2 μm pores in the membrane, the composite membrane cast from the vacuum process at 160 °C showed a dense structure with more uniformly distributed pores. The pore size for the vacuum dried composite membrane was ~ 0.8 μm (see inset figure). The morphology of the composite membrane slightly changed after phosphoric acid (PA) doping. The PA doped SnP_2O_7-Nafion composite has less porous structure as PA penetrated into the pores of the SnP_2O_7-Nafion composite structure (inset figure). The elongation of un-doped 90 wt% SnP_2O_7-Nafion composite was 15%, which further increased to 100% with additional PA doping (Fig. S5, ESI†).

Fig. 2b shows the proton conductivity of the 75 and 90 wt% SnP_2O_7-Nafion composite membranes and SnP_2O_7 pellet as a function of temperature. Substantially higher proton conductivity was obtained with the sample having higher SnP_2O_7 content. For example, the conductivity of un-doped 90 wt% SnP_2O_7-Nafion composite membrane was 40 mS cm^{-1} at 250 °C while the conductivity of un-doped 75 wt% SnP_2O_7-Nafion composite membrane was only 8 mS cm^{-1} at the same temperature. This is as expected since the Nafion used for the matrix material for the composite membrane does not have any

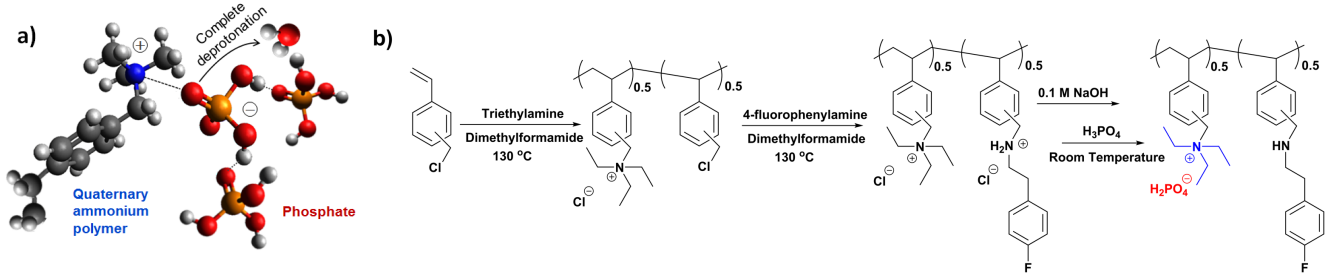

Fig. 3 (a) Schematic illustration for the interaction of quaternary ammonium polymer with phosphate molecules. (b) Synthetic procedure of phosphoric acid doped triethyl ammonium functionalized polystyrene.

measureable conductivity under dry conditions. The proton conductivity of the composite membranes was further improved with additional PA doping,[24] in which the P:M ratio was further increased from 3.50 to 4.64. The proton conductivity of the phosphoric acid doped 90 wt% SnP_2O_7-Nafion composite membrane was 62 mS cm^{-1} at 100 °C and reached 102 mS cm^{-1} at 290 °C. This indicates that the additional phosphate phase further facilitates the transport of protons. The stability of the additional phosphate phase in the composite membrane was evaluated by measuring the through-plane conductivity at 220 °C in a MEA configuration (Fig. 2c). The through-plane conductivity of the PA doped composite membrane was 60 mS cm^{-1}, ~14 % lower than the in-plane conductivity measured with the stand-alone membrane, probably due to higher contact resistance while measuring the through-plane conductivity. No notable changes in proton conductivity of the phosphoric acid doped composite membrane were observed over 500 h (Fig. S6, ESI†), indicating that the additional phosphate phase is stable.

Ion-pair Coordinated Ionomeric Binder

Optimal three-phase interface at the fuel cell electrodes plays a critical role in fuel cell performance. Most fuel cells using SnP_2O_7 particle electrolyte exhibited moderate fuel cell performance after electrolyte composition optimization, *ca.* peak power densities of 110 mW cm^{-2} and 190 mW cm^{-2} under H_2/O_2 at 240 °C for Pt/C (0.2 mg_{Pt} cm^{-2}) and Pt black (1 mg_{Pt} cm^{-2}) catalysts, respectively (Fig. S7a, ESI†). Electrodes prepared from direct vacuum Pt deposition[39] produced a better coverage of the electrolyte for Pt nanoparticles, thus the fuel cell performance was improved, *ca.* the peak power density of 150 mW cm^{-2} and 260 mW cm^{-2} at 220 °C for Pt/C (0.2 mg_{Pt} cm^{-2}) and Pt black (1 mg_{Pt} cm^{-2}) catalysts, respectively (Fig. S7b, ESI†). Adding polymeric Nafion binder in the electrodes improved the fuel cell performance further, particularly for MEAs with low Pt loading electrodes, *ca.* 190–230 mW cm^{-2} peak power densities for Pt/C (0.2 mg_{Pt} cm^{-2}) at 200 °C (Fig. S7c, ESI†). In spite of the performance improvement with several strategies for the electrode design, the peak power densities of all ITFCs were < 300 mW cm^{-2}, indicating an optimal three-phase interface was not achieved.

Our approach to achieving a better three-phase interface was to use a quaternary ammonium-biphosphate ion-pair coordinated polymer electrolyte instead of SnP_2O_7 particle or non-conducting polymeric binder. In the ion-pair coordinated system, the strong basicity of quaternary ammonium hydroxide causes complete deprotonation of phosphoric acid, enabling a strong ammonium cation-biphosphate anion ($H_2PO_4^-\cdots nH_3PO_4$) interaction (Fig. 3a).[41] With the ion-pair coordinated polymer, biphosphate-phosphoric acid complex conducts protons without water[42, 43], while ionic interaction with quaternary ammonium prevents the loss of the biphosphate phase at the ITFC operating temperature range. We synthesized a quaternary ammonium-biphosphate ion-pair coordinated polystyrene *via* nucleophilic substitution of trimethylamine and 4-fluorophethylamine onto poly(vinylbenzyl chloride) and subsequently doped it with 85 % phosphoric acid for 5 min at room temperature (Fig. 3b). The polyolefin backbone of the quaternary ammonium functionalized polystyrene provides inert environment for the electrochemical reaction, as a recent paper indicated that benzene adsorption on electrocatalysts significantly inhibits the hydrogen oxidation reaction.[44] The triethyl ammonium functional group instead of conventional trimethyl ammonium functional group may minimize the cationic group-catalyst interaction, which is beneficial to fuel cell durability.[45, 46]

Table 1. Properties of phosphoric acid doped quaternary ammonium (QA) functionalized polystyrene.

Conc. of QA (meq. g^{-1})	Number of phosphoric acid per QA [a]	Polymer content (%)	Proton conductivity (mS cm^{-1}) [b]
2.0	2.7	35	14

[a] obtained from acid-base titration
[b] measured at room temperature

The ^1H NMR spectra of the poly(vinylbenzyl chloride) and quaternized polystyrene confirmed that the intended structure was obtained (Fig. S8 ESI†). The ion exchange capacity of the quaternized polystyrene was 2.0 and the number of phosphate to ammonium is 2.7 (Table 1). The ion-pair coordinated polymer has good proton conductivity (14 mS cm^{-1}), consistent with the result found in the ammonium phosphate systems. The thermal stability of the quaternized and ion-pair coordinated polymer electrolytes was evaluated by thermogravimetric analysis. During the temperature scan from 90 to 800 °C under air, the major weight loss occurs in the three temperature ranges, i.e.

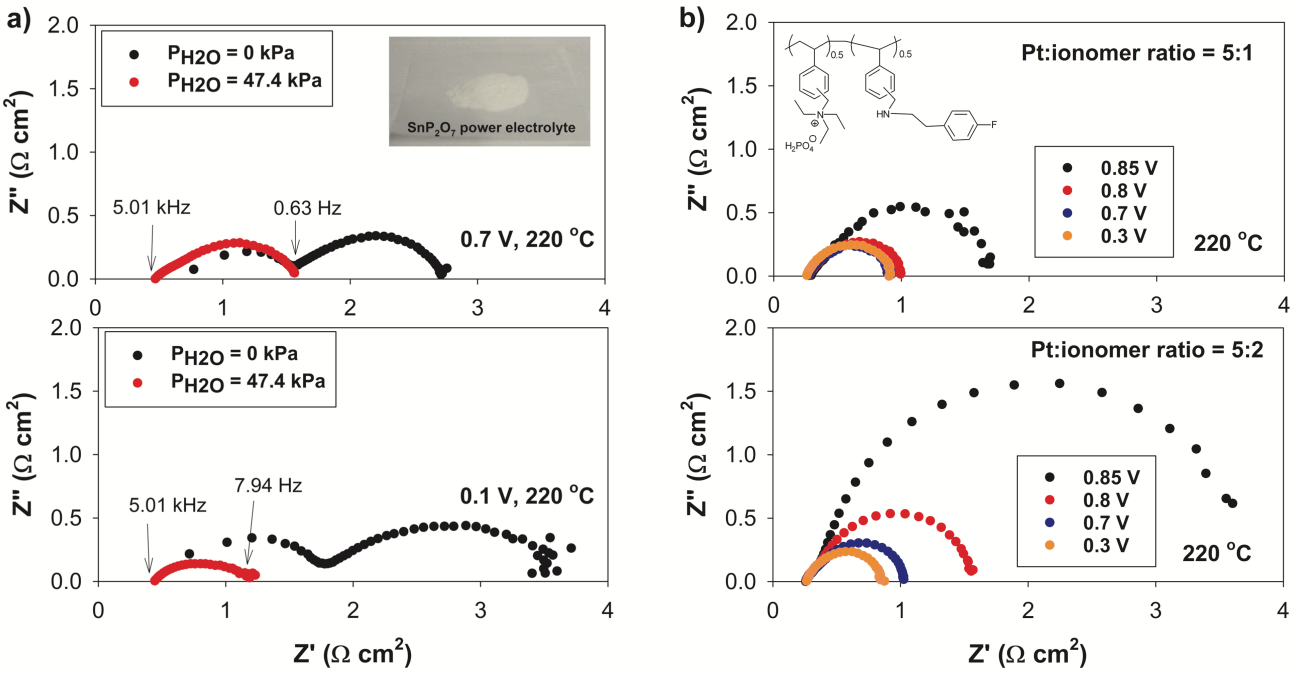

Fig. 4 EIS analysis of (a) SnP_2O_7 powder electrode; Pt black, 1 mg_{Pt} cm^{-2}, phosphoric acid doped 90 wt% SnP_2O_7/Nafion composite membrane (t = 100 μm) (b) ion-pair coordinated polymer electrode; Pt/C, 0.2 mg_{Pt} cm^{-2}, phosphoric acid doped 90 wt% SnP_2O_7/Nafion composite membrane (t = 80 μm). The EIS curves were obtained during H_2/O_2 fuel cell operations at 220 °C, 157 kPa backpressure.

200–400 °C, 350–450 °C and 500–700 °C (Fig. S9a, ESI†). While the first weight loss at 200–400 °C is due to the loss of phosphoric acid and water that have weak interactions with the ammonium groups, the weight loss at 350–450 °C and 500–700 °C correspond to the decomposition of ammonium group and polymer backbone degradation, respectively. It is interesting to note that the thermo-oxidative stability of the ion-pair coordinated polystyrene is higher than that of the un-doped quaternized polystyrene, in spite of the same chemical structure of the polymer. The increased thermal stability occurs because the ionic crosslinking induced from the ammonium-biphosphate ion pair enhances the thermo-oxidative stability of the polymer. In the isothermal test at 240 °C for ~350 hours, the ion-pair coordinated polymer electrolyte shows < 10% weight loss which is mostly due to the evaporation of loosely-bound phosphoric acid (Fig. S9b, ESI†).

The electrochemical impedance spectroscopy results (EIS) for the SnP_2O_7 particle electrode (Fig. 4a) and the ion-pair coordinated electrode (Fig. 4b) are compared. The MEA using SnP_2O_7 particle electrode under anhydrous operating conditions exhibits two semi-circles at high and low voltages. The first semi-circle in the high frequency region corresponds to the impedance associated with the charge transfer of the Pt catalysts. The second semi-circle in the low frequency region does not seem to be related with a diffusion-related term, as the second semi-circle did not disappear at the relatively high potential in which no diffusion-controlled process was involved. Instead this low frequency process is likely related with a secondary charge transfer resistance. When the MEA using the SnP_2O_7 particle electrode was slightly humidified (P_{H2O} = 47.4 kPa), the high frequency resistance decreased (due to the reduction of ohmic resistance of the membrane) and the low frequency semi-circle disappeared. This indicates that the low frequency second semi-circle is due to slower ionic transfer between SnP_2O_7 particles and Pt in the electrode. The MEA using the ion-pair coordinated electrode exhibited one semi-circle under anhydrous conditions and throughout all cell voltages. This suggests that the ion-pair coordinated polymer bonded electrode does not have the additional impedance originating from the ionic transfer observed in the SnP_2O_7 particle containing electrode or the diffusion-related impedance observed in LT-PEMFCs. Compared to the SnP_2O_7 particle containing electrode with P_{H2O} of 47.4 kPa, the ion-pair coordinated polymer electrode has significantly reduced low frequency impedance (0.58 Ω cm^2 for ion-pair *vs* 1.1 Ω cm^2 for SnP_2O_7), suggesting that the optimum three-phase interface was achieved with the ion-pair coordinated polymer electrode.

Fuel Cell Performance and CO Tolerance

The fuel cell performance of MEAs using 90 wt% SnP_2O_7/Nafion composite membrane (P:M = 4.64) and ion-pair coordinated polymer electrolyte in the electrodes was evaluated. Figure 5a shows the fuel cell performance at 200–240 °C with H_2 as fuel and O_2 as oxidant without humidification. The peak power density of 710–870 mW cm^{-2} was achieved at these operating temperatures with low cell high frequency resistance (HFR), *ca.* ~ 0.11 Ω cm^{-2}. The fuel cell performance was maintained for 3 days until the test was stopped. The high cell performance of the ITFC using the composite membrane and ion-pair coordinated polymer-bonded electrodes is attributed to (1) the

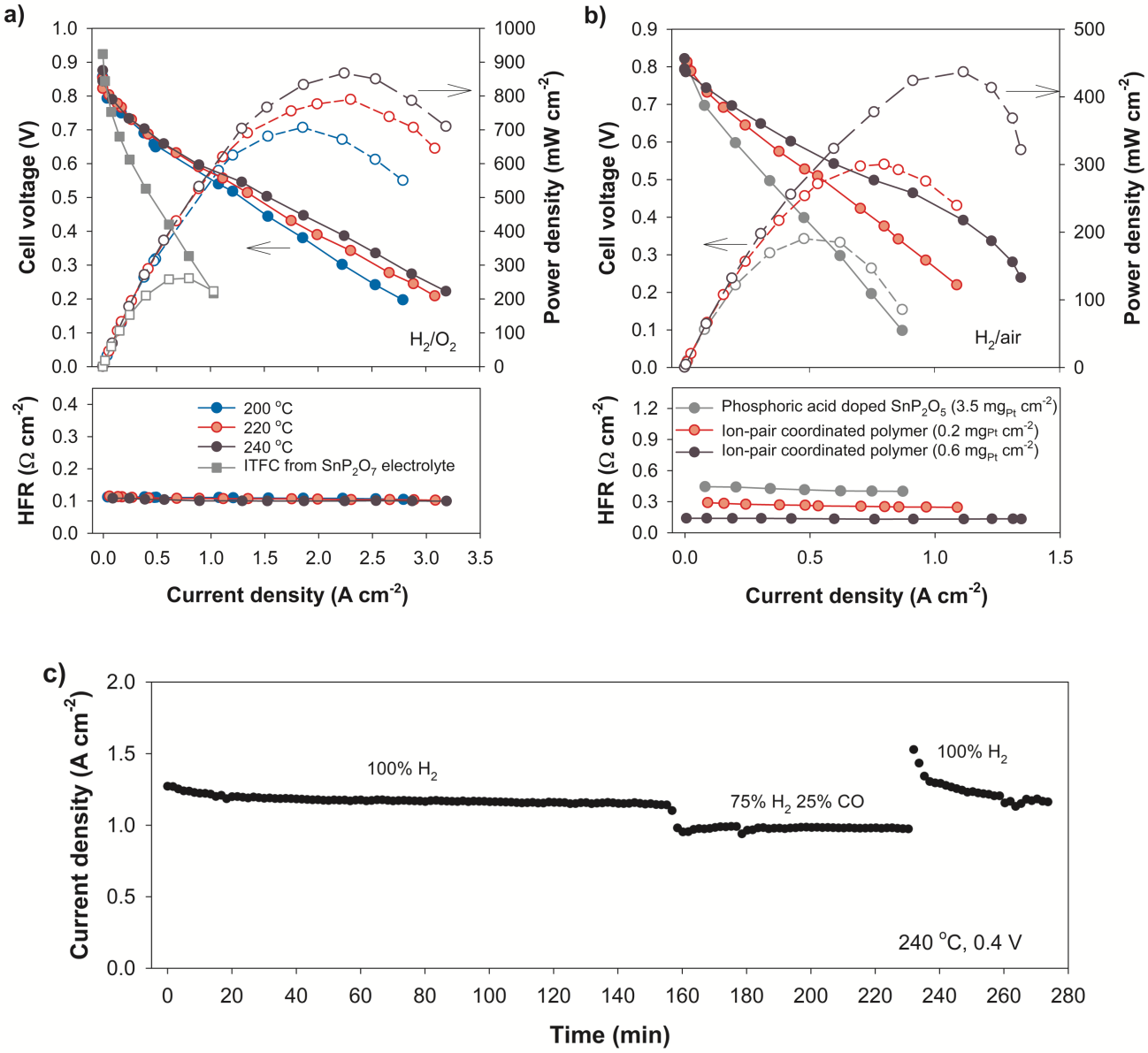

Fig. 5 (a) H_2/O_2 fuel cell performance with ion-pair coordinated polymer electrolyte; Pt/C (0.6 mg_{Pt} cm^{-2}), phosphoric acid doped 90 wt% SnP_2O_7/Nafion composite membrane (t = 80 μm) at 200–240 °C with 285 kPa backpressure. (b) H_2/air fuel cell performance comparison between ion-pair coordinated polymer electrolyte and phosphoric acid doped SnP_2O_7 electrolyte at 240 °C with 285 kPa backpressure; For the phosphoric acid doped SnP_2O_7, Pt/C (3.5 mg_{Pt} cm^{-2}) MEA, phosphoric acid doped 90 wt% SnP_2O_7/Nafion composite membrane (t = 120 μm) were used. For ion pair coordinated ionomers, Pt/C (0.2 mg_{Pt} cm^{-2}) and phosphoric acid doped 90 wt% SnP_2O_7 Nafion composite membrane (t = 120 μm) or Pt/C (0.6 mg_{Pt} cm^{-2}) and phosphoric acid doped 90 wt% SnP_2O_7/Nafion composite membrane (t = 80 μm) was used. (c) Fuel cell performance test using simulated reformate conditions (75% H_2 – 25% CO) versus O_2. Pt/C (0.6 mg_{Pt} cm^{-2}) and phosphoric acid doped 90 wt% SnP_2O_7/Nafion composite membrane (t = 100 μm) was used.

composite membrane providing good mechanical integrity to prevent reactant gas leakage and (2) the ion-pair coordinated electrolyte providing optimal three-phase interface without loss of phosphate phase. Fig. 5b compares the H_2/air fuel cell performance at two Pt loadings. With high Pt loading (0.6 mg_{Pt} cm^{-2}), the peak power density reached 410 mW cm^{-2} while with low Pt loading (0.2 mg_{Pt} cm^{-2}), the peak power density decreased to 300 mW cm^{-2} at 240 °C. Comparing this result to that of the MEA using SnP_2O_7 particle electrolyte and high Pt loading (3.5 mg_{Pt} cm^{-2}) which showed the peak power density of only 180 mW cm^{-2}, the performance improvement was substantial.

CO tolerance tests were conducted by supplying H_2 or a mixture of 25% CO and H_2 to the anode at 240 °C (Fig. 4c). The fuel cell current density was recorded at a constant voltage of 0.4 with pure H_2 and 25% CO over the course of 280 min

operation. It was observed that the current density slightly decreased from 1.14 to 1.0 A cm^{-2}, 12% loss, as 25% CO was introduced in the fuel stream. This example shows one benefit of the ITFCs over phosphoric acid doped PBI HT-PEMFCs which typically show 30–85% current density loss with 25% CO at the operating temperature of 140–180 °C.[47] The excellent CO tolerance indicates that the ITFC can be used for external reformer-based applications in which the CO concentration in the outlet gases can be up to 25%. Current reformer systems coupled with PEMFCs include water gas shift reactors to decrease the CO concentration to ≈1% and either a pressure swing adsorption system or preferential oxidation reactor for further decrease of the CO concentration to < 10 ppm. The introduction of these high performing ITFC can enable the use of a reformed hydrocarbon fuel directly from either a steam reformer or partial oxidation reactor.

Conclusions

We overcame two key technical barriers of ITFCs through the fabrication of a low resistance membrane separator and an optimal three-phase interface by rational design of a thermal resistant polymeric material. The ITFC using a SnP_2O_7-Nafion composite membrane and ion-pair coordinated polymer electrolyte-bonded electrodes showed excellent fuel cell performance under H_2/O_2, H_2/air and simulated reformate conditions, holding the promise of a high-performing anhydrous energy conversion device capable of operation at up to 250 °C. Research efforts toward further performance improvement of the ITFC are being made by mitigating the adverse effects of the adsorption of the phosphate anion[48] and phenyl group[49] on electrocatalyst surfaces. The intermediate temperature operation greatly simplifies thermal management and eliminates water management issues, thus dramatically simplifying the system and lowering costs. Implementing thermally stable polymers into ITFC components may be a viable way to open the practical use of ITFC in various systems which require non-precious metal or low loading of precious metal catalysts, impurity tolerance, and the direct use of liquid fuel alternatives.

Experimental

Materials

Nafion membranes (NR-212, 50 μm thickness) were purchased from Ion Power, Inc. (USA). Pt/C (60%, HiSPEC® 9100), Pt/C (20%, HISPEC® 3000), and Pt black (HISPEC® 1000) were purchased from Alfa Aesar (USA). Single-side ELAT® gas diffusion layers (GDLs) were obtained from ETEK (USA). $SnCl_4$, diammonium phosphate, silicon carbide nanowhisker, Poly(vinylbenzyl chloride) (PS-bzCl), trimethylamine (TEA), 4-fluorophenethylamine, 1,2-pentanediol, *N,N*-dimethylformamide (DMF), and phosphoric acid (85 wt% in H_2O) were purchased from Sigma-Aldrich and used without further purification.

SnP_2O_7 Particle Synthesis

6.2 g of $SnCl_4$ hydrate was dissolved in 30 g of alcohol, to which 10.1 g diammonium phosphate dissolved in 12.2 g of hot H_2O was quickly added with vigorous stirring. The mixture was heated and evaporated with continued stirring until thickening, then removed from heat. Cooling resulted in a thick "frosting" that was dried at 60 °C. The foamy mass was fired in a covered crucible at 650 °C for 2.5 hours. The product was dry-milled with zirconia balls to form a fine powder.

Fabrication of SnP_2O_7 Pellet

SnP_2O_7 powder was thoroughly mixed with 15 wt% nanowhisker and hot-pressed at 230 °C and 315 MPa in a 12.7 mm diameter pellet die to form a 0.25 mm thick pellet. The silicon carbide used as nanowhiskers to prevent cracking in SnP_2O_7 pellets owing to its affinity towards phosphates and stability in phosphoric acid. Before conductivity measurement, the SnP_2O_7 pellet was sandwiched between two phosphoric acid doped gas diffusion electrodes (GDEs, 10 mg_{Pt} cm^{-2}).

Preparation of SnP_2O_7-Polymer Composite Membrane

The Nafion 212 (H^+ form) membrane was converted to Na^+ form by immersing in the boiling 2% NaOH solution for 1 hour and subsequent rinsing with deionized water for 1 hour. The membrane was dried at 60 °C for 30 min before dispersing in 1,2-pentanediol at 140 °C for 2 hours. SnP_2O_7 powder was mixed in the 5 wt% Nafion dispersion with the aid of tip ultra-sonicator. The SnP_2O_7/Nafion mixture was cast on the clean glass plate at the 120 °C for 3 hours and further dried in the vacuum (−90 kPa) at 160 °C for 4 hours. Alternatively, SnP_2O_7/Nafion mixture was cast at 140 °C/4 hours and subsequent dry at 190 °C/4 hours under ambient pressure conditions. For further phosphoric acid doping, the composite membrane was immersed into 85 % phosphoric acid for 3 hours at room temperature.

Synthesis of Ion-pair Coordinated Polystyrenes

The quaternary ammonium hydroxide tethered polystyrene ionomeric binder was synthesized *via* nucleophilic substitution of TEA and 4-fluorophenethylamine onto PS-bzCl. A solution of 10 g of PS-bzCl in DMF (360 ml) was reacted with 3.32 g of TEA at 130 °C for 3 hours. To the reaction mixture, 4.56 g of 4-fluorophenethylamine was added and reacted for an additional 12 hours. This 5 wt% polystyrene copolymer solution in DMF was used as an ionomer solution.

Proton Conductivity Measurements

In-plane proton conductivity of the composite membranes was measured from AC impedance spectroscopy using a Solartron 1260 gain phase analyser over a frequency range from 1 MHz to 1 Hz. Sample strips had dimensions of approximately 0.5 × 1 inch and were placed between two Pt coated electrodes of a window cell. The window cells were connected to the AC impedance analyser and placed in convection oven to control temperature. The in-plane conductivity (σ, S cm^{-1}) of the

composite membranes in the longitudinal direction was calculated from the equation:

$$\sigma = \frac{L}{R \times d \times W} \quad (1)$$

where *L* (cm) is the distance between the electrodes *R* (Ω) is the resistance that was read from the low intersect of the high-frequency semicircle on a complex impedance plane with the Re (*Z*) axis, *d* (cm) is the thickness of the membrane, and *W* (cm) is the width of the membrane.

Through-plane proton conductivity of the composite membranes was measured using fuel cell hardware. Composite membranes were sandwiched between two Pt-coated GDEs which were pressed on the composite membrane in the fuel cell hardware. The HFR (Ω cm^2) of the cell was measured from AC impedance spectroscopy over a frequency range from 1 MHz to 1 Hz. Area specific resistance (ASR) was calculated from the equation:

$$ASR = HFR - R_{CC} - R_{FF} - R_{GDE} \quad (2)$$

where R_{CC}, R_{FF}, and R_{GDE} are resistance of current collector, flow field and GDE, respectively. The summation of the component resistance was measured to 29.4 mΩ cm^2.[50] The through-plane conductivity was obtained from the equation:

$$\sigma = \frac{t}{ASR} \quad (3)$$

Fabrication of Membrane Electrode Assembly

Electrodes using SnP_2O_7 particle (3.5 mg_{Pt} cm^{-2}) were prepared from the catalyst ink comprised of 35 mg Pt black, 35 mg of SnP_2O_7, 70 mg of water and 350 mg of n-propanol. Nafion bonded SnP_2O_7 electrodes (0.2 mg_{Pt} cm^{-2}) were prepared from the catalyst ink consist of 10 mg of 20% Pt/C, 40 mg of 5 wt% Nafion dispersion, 20 mg of 10 wt% SnP_2O_7 dispersion in 1,2-pentanediol and 1,000 mg of 1,2-pentanediol. For ion-pair coordinated polymer electrodes (0.6 or 0.2 mg_{Pt} cm^{-2}), 10 mg of 60% Pt/C or 20% Pt/C were ultrasonically mixed with the calculated amount of quaternary ammonium tethered poly(styrene) hydroxide ionomer in methanol/ethylene glycol mixture as described elsewhere.[41] The catalyst inks were sonicated with tip ultrasonicator for homogenous solution. GDEs were prepared by painting catalyst inks directly onto GDLs (5 cm^2) on a vacuum plate at 100 °C or 140 °C for SnP_2O_7 particle, ion-pair coordinated polymer or Nafion bonded SnP_2O_7 electrodes, respectively. Prior to assembly, the polymer-bonded electrodes were immersed in the 85% phosphoric acid for 5 minutes. Then, the phosphoric acid doped composite membrane was sandwiched by two electrodes to yield the MEAs.

Fuel Cell Characterization

H_2/O_2 (or air) fuel cell performance of the MEAs was measured using a fuel cell test station (Fuel Cell Technologies, Inc.). Polarization curves and HFR of MEAs were obtained at temperatures ranging from 200 to 240 °C. H_2 and O_2 (or air) were supplied at a rate of 200 and 300 (or 500) sccm, respectively. The HFR of the cell was measured while obtaining the polarization curve. In order to choose the frequency that minimizes the capacitance, a sinusoidal wave perturbation between 2 and 10 kHz was applied to the fuel cell load before obtaining polarization curves. The same conditions were used for generating EIS, obtained under 10 mA of amplitude from 10 k Hz to 1 Hz of frequency at the cell voltage range of 0.85–0.1 V. The For long-term stability tests, current density at a constant voltage was measured every minute. The CO tolerance testing was performed using 25 cm^2 fuel cell hardware by feeding 25 wt% CO in the H_2 stream. The current density at a constant voltage of 0.4 V was measured at 240 °C as a function of time.

Acknowledgements

We thank Dr. Alex Papandrew (University of Tennessee Knoxville) for providing direct vacuum Pt deposited electrodes. This work was supported by the U.S. Department of Energy, the Advanced Research Project Agency-Energy (ARPA-E) program (Award number: DE-AR0000314). Los Alamos National Laboratory is operated by Los Alamos National Security, LLC under Contract DE-AC52-06NA25396.

Notes and references

1. N. Jayaprakash, J. Shen, S. S. Moganty, A. Corona and L. A. Archer, *Angew Chem Int Ed*, 2011, **123**, 6026-6030.
2. Y. Zhu, Y. Yin, X. Yang, T. Sun, S. Wang, Y. Jiang, J. Yan and X. Zhang, *Angew Chem Int Ed*, 2017, **56**, 7881-7885.
3. Q. Liu, T. Liu, D. Liu, Z. Li, X. Zhang and Y. Zhang, *Adv Mater,* 2016, **28**, 8413-8418.
4. C. H. Park, S. Y. Lee, D. S. Hwang, D. W. Shin, D. H. Cho, K. H. Lee, T. W. Kim, T. W. Kim, M. Lee, D. S. Kim, C. M. Doherty, A. W. Thornton, A. J. Hill, M. D. Guiver and Y. M. Lee, *Nature*, 2016, **532**, 480-483.
5. S. Gottesfeld, D. R. Dekel, M. Page, C. Bae, Y. Yan, P. Zelenay and Y. S. Kim, *J. Power Sources*, 2018, **375**, 170-184.
6. L. X. Xiao, H. F. Zhang, E. Scanlon, L. S. Ramanathan, E. W. Choe, D. Rogers, T. Apple and B. C. Benicewicz, *Chem Mater*, 2005, **17**, 5328-5333.
7. C. C. Duan, J. H. Tong, M. Shang, S. Nikodemski, M. Sanders, S. Ricote, A. Almansoori and R. O'Hayre, *Science*, 2015, **349**, 1321-1326.
8. T. Hibino, A. Hashimoto, T. Inoue, J. Tokuno, S. Yoshida and M. Sano, *Science*, 2000, **288**, 2031-2033.
9. E. D. Wachsman and K. T. Lee, *Science*, 2011, **334**, 935-939.
10. J. M. Moore, P. L. Adcock, J. B. Lakeman and G. O. Mepsted, *J Power Sources*, 2000, **85**, 254-260.
11. Q. F. Li, R. H. He, J. O. Jensen and N. J. Bjerrum, *Chem Mater*, 2003, **15**, 4896-4915.
12. D. A. Boysen, T. Uda, C. R. I. Chisholm and S. M. Haile, *Science*, 2004, **303**, 68-70.
13. S. M. Haile, D. A. Boysen, C. R. I. Chisholm and R. B. Merle, *Nature*, 2001, **410**, 910-913.
14. P. Bocchetta, G. Chiavarotti, R. Masi, C. Sunseri and F. Di Quarto, *Electrochem Commun*, 2004, **6**, 923-928.
15. T. Matsui, T. Kukino, R. Kikuchi and K. Eguchi, *J Electrochem Soc*, 2006, **153**, A339-A342.

16. M. Nagao, A. Takeuchi, P. Heo, T. Hibino, M. Sano and A. Tomitab, *Electrochem Solid State Lett*, 2006, **9**, A105-A109.
17. M. Nagao, T. Kamiya, P. Heo, A. Tomita, T. Hibino and M. Sano, *J Electrochem Soc*, 2006, **153**, A1604-A1609.
18. X. F. Sun, S. R. Wang, Z. R. Wang, X. F. Ye, T. L. Wen and F. Q. Huang, *Solid State Ionics*, 2008, **179**, 1138-1141.
19. G. Alberti, M. Casciola, S. Cavalaglio and R. Vivani, *Solid State Ionics*, 1999, **125**, 91-97.
20. Y. Z. Li, T. Kunitake, Y. Aoki and E. Muto, *Adv Mater*, 2008, **20**, 2398-2404.
21. S. Yoshimi, T. Matsui, R. Kikuchi and K. Eguchi, *J Power Sources*, 2008, **179**, 497-503.
22. Y. C. Jin, Y. B. Shen and T. Hibino, *J Mater Chem*, 2010, **20**, 6214-6217.
23. G. Harley, K. D. Kreuer, J. Maier and L. C. De Jonghe, *J Non-Cryst Solids*, 2009, **355**, 932-937.
24. S. R. Phadke, C. R. Bowers, E. D. Wachsman and J. C. Nino, *Solid State Ionics*, 2011, **183**, 26-31.
25. S. W. Tao, *Solid State Ionics*, 2009, **180**, 148-153.
26. Y. Sato, Y. B. Shen, M. Nishida, W. Kanematsu and T. Hibino, *J Mater Chem*, 2012, **22**, 3973-3981.
27. X. X. Xu, S. W. Tao, P. Wormald and J. T. S. Irvine, *J Mater Chem*, 2010, **20**, 7827-7833.
28. C. R. Kreller, H. H. Pham, M. S. Wilson, R. Mukundan, N. Henson, M. Sykora, M. Hartl, L. Daemen and F. H. Garzon, *J Phys Chem C*, 2017, **121**, 23896-23905.
29. C. R. Kreller, M. S. Wilson, R. Mukundan, E. L. Brosha and F. H. Garzon, *Ecs Electrochem Lett*, 2013, **2**, F61-F63.
30. Z. L. Chai, Q. Y. Suo, H. Wang and X. J. Wang, *Rsc Adv*, 2013, **3**, 21928-21935.
31. T. J. Omasta, A. M. Park, J. M. LaManna, Y. Zhan, X. Peng, L. Wang, D. L. Jacobson, J. R. Varcoe, D. S. Hussy, B. S. Pivovar and W. E. Mustain, *Energy Environ Sci*, 2018, DOI: 10.1039/C8EE00122G.
32. X. Zhu, H. Zhang, Y. Zhang, Y. Liang, X. Wang and B. Yi, *J Phys Chem B,* 2006, **110**, 14240-14248.
33. J. Li, X. Li, Y. Zhao, W. Lu, Z. Shao and B. Yi, *ChemSusChem*, 2012, **5**, 896-900.
34. J. Yan, H. Matsumoto, M. Enoki and T. Ishihara, *Electrochem. Solid State Lett,* 2005, **8**, A389-A391.
35. T. Uda and S. M. Haile, *Electrochem Solid State Lett*, 2005, **8**, A245-A246.
36. Y. C. Jin, K. Fujiwara and T. Hibino, *Electrochem Solid St*, 2010, **13**, B8-B10.
37. G. Qing, R. Kikuchi, A. Takagaki, T. Sugawara and S. T. Oyama, *J Electrochem Soc*, 2014, **161**, F451-F457.
38. O. Paschos, J. Kunze, U. Stimming and F. Maglia, *J Phys Condens Matter*, 2011, **23**, 234110.
39. A. B. Papandrew, C. R. I. Chisholm, R. A. Elgammal, M. M. Ozer and S. K. Zecevic, *Chem Mater*, 2011, **23**, 1659-1667.
40. Y. S. Kim, C. F. Welch, R. P. Hjelm, N. H. Mack, A. Labouriau and E. B. Orler, *Macromolecules*, 2015, **48**, 2161-2172.
41. K.-S. Lee, J. S. Spendelow, Y. K. Choe, C. Fujimoto and Y. S. Kim, *Nature Energy*, 2016, **1**, 16120.
42. K. D. Kreuer, *Chem Mater*, 2014, **26**, 361-380.
43. K. Kluy, B.B.L. Reeb, O. Paschos, F. Maglia, O. Schneider, U. Stimming, S. Angioni, P.P. Righetti, *ECS Trans*, 2012, **50**, 1255-1261.
44. I. Matanovic, H. T. Chung and Y. S. Kim, *J Phys Chem Lett*, 2017, **8**, 4918-4924.
45. H. T. Chung, U. Martinez, J. Chlistunoff, I. Matanovic and Y. S. Kim, *J Phy Chem Lett*, 2016, **7**, 4464-4469.
46. H. Chung, Y. K. Choe, U. Martinez, I. Gonzalez, A. Mohanti, C. Bae and Y. S. Kim, *J Electrochem Soc*, 2016, **163**, F1503-F1509.
47. A. D. Modestov, M. R. Tarasevich, V. Y. Filimonov and E. S. Davydova, *Electrochim Acta*, 2010, **55**, 6073-6080.
48. Q. C. He, X. F. Yang, W. Chen, S. Mukerjee, B. Koel and S. W. Chen, *Phy Chem Chem Phy,* **12**, 2010, 12544-12555.
49. I. Matanovic, H. T. Chung and Y. S. Kim, *J Phys Chem Lett,* 2017, **8**, 4918-4924.
50. B. S. Pivovar and Y. S. Kim, *J Electrochem Soc*, 2007, **154**, B739-B744.